A flux-limiting wetting-drying method for finite-element shallow-water models, with application to the Scheldt Estuary

Olivier Gourgue*, Richard Comblen, Jonathan Lambrechts,
Tuomas Kärnä, Vincent Legat and Eric Deleersnijder

Université catholique de Louvain, Centre for Systems Engineering and Applied Mechanics (CESAME). 4, Avenue Georges Lemaître. B-1348 Louvain-la-Neuve, Belgium.

Manuscript submitted to *Advances in Water Resources*.
September 9, 2009

Abstract

We present a flux-limiting wetting-drying approach for finite element discretizations of the shallow water equations using discontinuous linear elements for the elevation. The key ingredient of the method is the use of limiters for generalized nodal fluxes. This method is implemented into the Second-generation Louvain-la-Neuve Ice-ocean Model (SLIM), and is verified against standard test cases. The method is further applied to the wetting and drying of sand banks in the Scheldt Estuary, which is located in northern Belgium and the sourthern Netherlands. The results obtained for both the benchmarks and the realistic problem illustrate the accuracy of the method in describing the hydrodynamics in the vicinity of dry areas. In particular, the method strictly conserves mass, and there is no transport through dry areas.

Key words: wetting-drying, tidal flat, estuary, Scheldt, finite element, discontinuous Galerkin.

---

* Corresponding author. E-mail: olivier.gourgue@uclouvain.be. Tel: +32 10 47 23 60. Fax: +32 10 47 21 80.

1 Introduction

Most of the world's coastal seas are linked to embayments, estuaries and lagoons. A large number of these shallow water bodies experience tidal oscillations of the free surface. Consequently, the extent of areas subject to alternating wetting and drying (the so-called tidal flats) can be as large as the permanently-submerged areas. The influence of the tidal flats is therefore of a crucial importance, so the wetting and drying processes need to be accurately simulated. Furthermore, tidal flats play a very important role in the ecosystem of these areas. The ability to represent the wetting and drying processes is thus a key feature in coastal eco-hydrodynamic modeling.

The wetting-drying methods can be classified into two main categories: the deformed mesh or Lagrangian methods and the fixed mesh or Eulerian methods. Early studies showed the potential of the deformed mesh strategy [52, 44], where the nodes on the boundary between wet and dry zones move following the front. But since the nodal coordinates vary at each time step, an important part of the model is devoted to the mesh adaptation, making this approach rather expensive. Consequently, it was mostly restricted to idealized test cases [16, 48], while the Eulerian fixed mesh strategy has been much widely used in realistic applications. The Eulerian methods can also be divided into two main approaches: the flux-limiting methods and the so-called modified equation methods. With the flux-limiting strategy, only the discrete algebraic form of the hydrodynamic equations is modified. With the modified equation strategy, the original continuous form of the partial differential equations is modified.

The earliest flux-limiting method was suggested by Leendertse [42] for a two-dimensional finite difference model. This type of approach turns off/on the mesh cells when the water thickness rises below/above a threshold value, limiting or cancelling out the water fluxes on dry cells in order for the water depth to remain positive. However, an artificial slope of the free surface is formed in the dry areas because the water level is arbitrarily fixed at the bed elevation. This generates an extra pressure gradient term, which may lead to unstable behavior and has to be treated specifically. Nevertheless, this flux-limiting approach proved very popular in two-dimensional [7] and three-dimensional [43, 33, 63, 47, 1] finite difference models. The review of Balzano [7] is particularly extensive, gathering ten different methods. The flux-limiting approach is also popular in finite volume modeling [8, 14, 59]. However, there are only a few examples of finite element models using such a method [41].

The first method among the modified equation approach is the porosity method [31, 26], in which the hydrodynamic equations are modified to allow water flow in a porous layer below the bed. The water depth can therefore be negative. This method avoids handling separately dry or wet cells, but allows unphysical water fluxes through dry zones. Therefore, the total mass of water within wet areas is not constant in time and conservation is then only ensured in a weak sense. Another objection to the

porosity method is the lack of physical description of the so-called porous layer. It is no more the case with the capillary method that uses capillarity effect properties to describe wetting and drying processes [55, 34]. Finally, the last method among the modified equation approach is the damping or kinematic method. The processes like rotation and advection are neglected when the water column becomes very shallow such that a simple balance between external pressure gradient and friction prevails [32, 13, 25]. However, ensuring that the water depth remains positive by modifying the equations leads to spurious mass flux through dry areas.

The selection of the suitable Eulerian method is difficult and in fact should depend on the flow under study. The problem to be tackled is highly nonlinear. Therefore, implicit time-stepping schemes are difficult to implement. The modified equation approach has a straightforward linearization that enables the use of a semi-implicit time-stepping. However it may lead to strong unphysical water fluxes, especially when using large time steps. Iterative solutions can be considered for both methods, but the convergence of such schemes requires the use of rather small time steps. In this paper, we focus on explicit time-stepping. As explicit methods are involved, the flux-limiting approach has the great advantage that the physics is not modified in the vicinity of dry areas.

The objective of this paper consists in developing a new flux-limiting finite-element method for the shallow water equations that uses discontinuous linear elements for the elevation. This method is implemented within the **S**econd-generation **L**ouvain-la-Neuve **I**ce-ocean **M**odel (SLIM[1]). The discontinuous finite element method appears to be very attractive for solving shallow water flows [3, 51, 49, 21, 4]. It combines advantages of both continuous finite element methods and finite volumes. It is known to be especially efficient for hyperbolic conservation laws [18], and robust solutions are known to handle second-order diffusive operators [6, 50]. Due to the discontinuous character of the solution, degrees of freedom are not shared between elements. Parallel implementation is then straightforward, and h- and p-adaptation procedures can be easily designed, as an accurate error estimator is simply given by the inter-element jumps of the solution [15, 9]. High order version of the scheme can be defined [46, 28], requiring equally accurate description of the geometry [11], and giving excellent dispersive and dissipative behavior [2, 10]. Efficient slope limiters allow for the design of shock capturing version of the scheme [17, 36, 15].

This paper is structured as follows. The shallow water equations, the wetting-drying method and the model in which it is implemented are described in Section 2. Next, in order to verify the method, the results obtained on the Balzano, Leclerc and Thacker test cases are shown in Section 3. The modeling of the wetting and drying processes occuring in the Scheldt Estuary is then presented in Section 4. Finally, conclusions are drawn in Section 5.

[1] http://www.climate.be/SLIM

2 Basic equations and numerical techniques

The shallow water equations are obtained from the incompressible Navier-Stokes equations by assuming that the pressure is in hydrostatic balance and that the density of the fluid is constant, and by averaging the equations along the vertical direction. Coastal flows are well represented by those equations if the water column is well mixed. The convective formulation of the shallow water equations reads:

$$\frac{\partial \eta}{\partial t} + \boldsymbol{\nabla} \cdot \Big((h+\eta)\ \boldsymbol{u} \Big) = 0\ , \tag{1}$$

$$\frac{\partial \boldsymbol{u}}{\partial t} + \big(\boldsymbol{u} \cdot \boldsymbol{\nabla}\big)\boldsymbol{u} + f\boldsymbol{k} \times \boldsymbol{u} + g\boldsymbol{\nabla}\eta = \frac{1}{H}\boldsymbol{\nabla} \cdot \Big(H\nu\big(\boldsymbol{\nabla}\boldsymbol{u}\big)\Big) + \frac{\boldsymbol{\tau}^s - \boldsymbol{\tau}^b}{\rho H}\ , \tag{2}$$

where t is the time and $\boldsymbol{\nabla}$ is the horizontal gradient operator; η is the elevation of the free surface above a reference level, and $\boldsymbol{u}$ is the horizontal velocity vector averaged over the water column; η and $\boldsymbol{u}$ are the state variables that depend on time and position; $H = h + \eta$ is the actual water depth, where h is the reference height of the water column; $f = 2\omega \sin\phi$ is the Coriolis parameter, where ω is the angular velocity of the Earth and ϕ is the latitude, and $\boldsymbol{k}$ is the unit upward vector; g is the gravitational acceleration; ν is the horizontal eddy viscosity; $\boldsymbol{\tau}^s$ and $\boldsymbol{\tau}^b$ are the surface and bottom stress vectors, respectively, and ρ is the density of water. This formulation can be related to any coordinate system, when the horizontal plan is defined as normal to the gravity. In what follows, we always refer to $\boldsymbol{u}$ as the velocity vector, omitting the reference to the average over the water column.

In order to obtain a well-posed problem, suitable boundary conditions have to be imposed along the boundary of the domain. Including viscosity or not will change the number of required boundary conditions [58]. Finally, an initial state has to be provided. However, due to frictional and viscous dissipation, and, in some cases, to open boundary conditions, its influence becomes negligible after some time. So any arbitrary initial condition can be considered for long term simulations.

A major issue for the shallow water equations in coastal modeling is their inability to deal with dry areas, where the water height is theoretically zero. The role of a wetting-drying method is to allow the appearance and disappearance of dry areas. The aim of this paper is to describe and verify a wetting-drying method that modifies neither the mesh nor the original form of the continuous equations. Such a wetting-drying method is classified among the flux-limiting methods.

The present wetting-drying method is designed for finite element models using P_1^{DG} elements for the elevation field. In other words, the elevation η is approximated by discontinuous piecewise-linear surfaces on triangles. The computational domain Ω is therefore divided into a set of M triangular elements Ω_e, forming the mesh. The first interesting property is the linear character of the P_1^{DG} elements. It implies a monotonic shape of the elevation field on each element. The smallest value among the three nodes is the smallest value throughout the triangle. A triangle with three wet

nodes is therefore wet everywhere. This is not the case with higher order elements. The second interesting property is the discontinuous character of the P_1^{DG} elements. It requires no inter element continuity, and information can only pass from an element to its neighbor through fluxes that can easily be turned on/off.

The present wetting-drying method mainly deals with the mass conservation equation (1), which can be rewritten as:

$$\frac{\partial \eta}{\partial t} = \underbrace{-\boldsymbol{\nabla} \cdot \Big((h+\eta)\ \boldsymbol{u} \Big)}_{F(\eta, \boldsymbol{u})} . \tag{3}$$

According to the nature of the equation, the operator F is conservative: its integral is zero over the whole domain Ω, if the latter is closed. The method is divided in three main steps that are illustrated on Figure 1 and detailed below. The elevation at time step n (η^n) is known before starting the wetting-drying method. Each step of the method corresponds to an intermediate elevation (η^*, η^{**} and η^{***}). The elevation at time step $n+1$ (η^{n+1}) is then found.

- In the first intermediate step, corresponding to η^*, the elevation is clipped to ensure that the water depth $h+\eta^*$ is not smaller than the threshold value H_{dry} at each position:

$$\eta^* = \max\left(\eta^n, H_{\text{dry}} - h\right) . \tag{4}$$

- In the second intermediate step, corresponding to η^{**}, the equation (3) is used with $\eta = \eta^*$ to ensure that only positive water depths are involved:

$$\frac{\eta^{**} - \eta^n}{\Delta t} = F(\eta^*, \boldsymbol{u}) . \tag{5}$$

  Since the operator F is conservative, the mass is conserved between the second intermediate state ($**$) and the initial state (n). The problem with the second intermediate state is that the free surface may have moved down in already dry areas.

- In the third intermediate step, corresponding to η^{***}, the operator F is modified to ensure that the free surface does not move down in dry areas while remaining conservative:

$$\frac{\eta^{***} - \eta^n}{\Delta t} = F^*(\eta^*, \boldsymbol{u}) . \tag{6}$$

  The third intermediate state represents accurately the water level around dry areas.

In practice, η^{**} and η^{***} are not computed. The second intermediate step only consists in building F, and the third intermediate step only consists in modifying it into F^*.

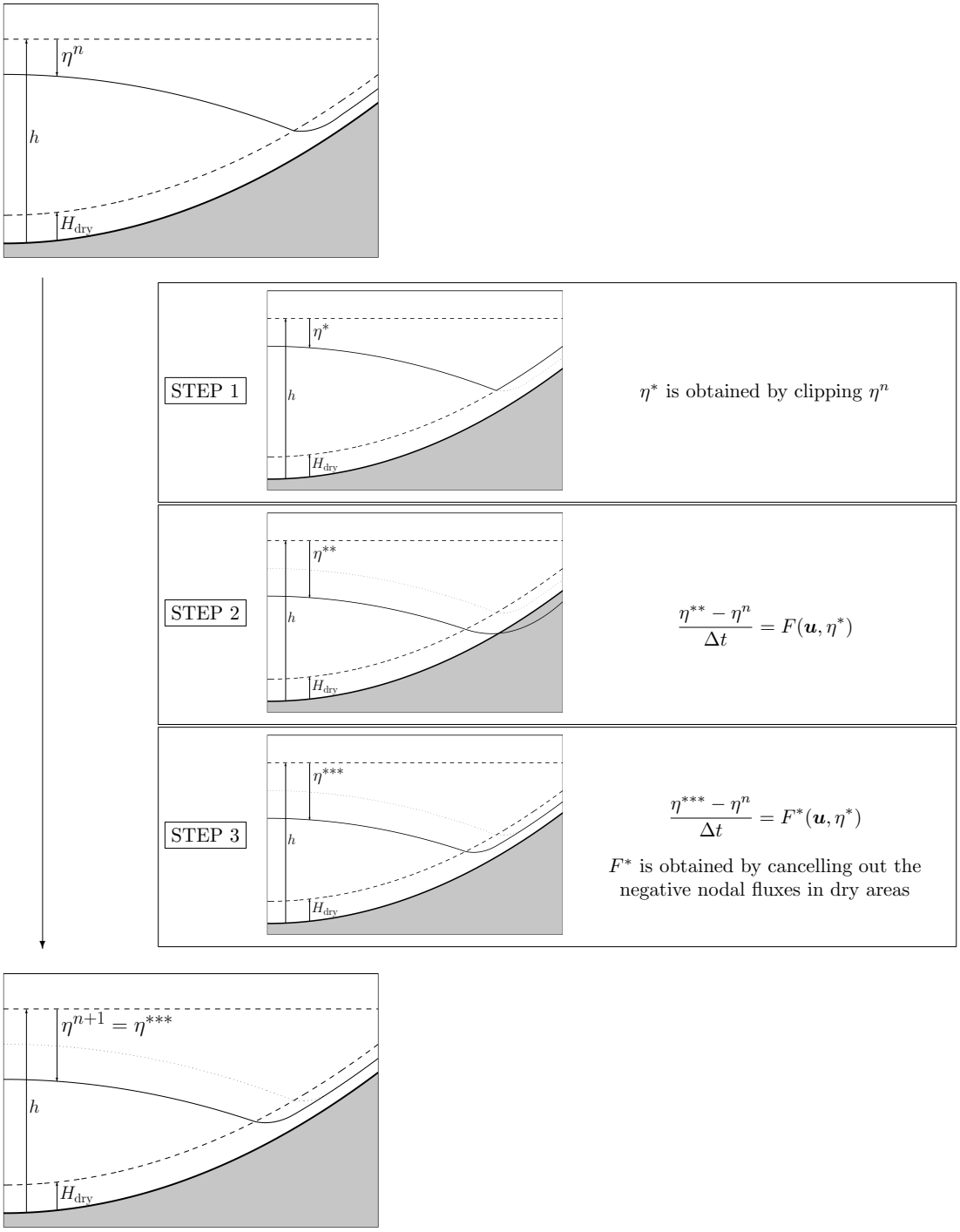

Figure 1: Illustration of the three steps of the wetting-drying method and the corresponding intermediate states of the elevation.

The elevation at time step $n+1$ is then computed as follows:

$$\frac{\eta^{n+1}-\eta^n}{\Delta t} \quad = \quad F^*\big(\eta^*, \boldsymbol{u}\big) \ . \tag{7}$$

In order to describe how F is modified to obtain the operator F^* in the third intermediate step, the weak and discrete formulations of equation (5) need to be detailed. Because the method is designed for discontinuous elements, the weak formulation can be written for each element. In what follows, the wetting-drying method is described for only one triangle Ω_e. The method needs to be repeated for each triangle of the whole domain. The weak formulation is found by multiplying equation (5) by a test function $\hat{\eta}$ and integrating it over Ω_e. Integrating by parts the operator F and using the divergence theorem leads to

$$< \hat{\eta} \ \frac{\eta^{**}-\eta^n}{\Delta t} \ >_e = \ - \ll \hat{\eta} \ (h+\eta^*) \ \boldsymbol{u}\cdot\boldsymbol{n} \gg_e + < \big(\boldsymbol{\nabla}\hat{\eta}\big)\cdot\big((h+\eta^*) \ \boldsymbol{u}\big) >_e \ , \tag{8}$$

where $< \cdot >_e$ and $\ll \cdot \gg_e$ refer to the integral over the element Ω_e and along the boundary $\partial\Omega_e$ of this element, respectively, and $\boldsymbol{n}$ is the outward unit vector normal to $\partial\Omega_e$.

Because the method deals with linear elements, the approximation of the field η is

$$\eta = \sum_{j=1}^{3} \eta_j \phi_j \quad \triangleq \quad \eta_j \phi_j \ , \tag{9}$$

where η_j is the nodal value of the field η at node j and ϕ_j is the corresponding linear shape function. Following the Einstein convention, the summation symbol is removed for the repeated indices. The discrete formulation of equation (8) is obtained by replacing η by its approximation in the left-hand side of the equation, and by taking any shape function ϕ_i as test function:

$$\underbrace{< \phi_i \phi_j >_e}_{A_{ij}} \ \frac{\eta_j^{**}-\eta_j^n}{\Delta t} \quad = \quad \underbrace{- \ll \phi_i \ (h+\eta^*) \ \boldsymbol{u}\cdot\boldsymbol{n} \gg_e}_{b_i^c\left(\boldsymbol{u},\eta^*\right)} + \underbrace{< \big(\boldsymbol{\nabla}\phi_i\big)\cdot\big((h+\eta^*) \ \boldsymbol{u}\big) >_e}_{b_i^s\left(\boldsymbol{u},\eta^*\right)} \ , \tag{10}$$

where $i = 1 \ ... \ 3$. Let $\left(A^{-1}\right)_{ij}$ be the inverse of A_{ij}. The equation (11) may be rewritten as

$$\frac{\eta_j^{**}-\eta_j^n}{\Delta t} \quad = \quad \underbrace{\left(A^{-1}\right)_{ji} \ b_i^c\big(\boldsymbol{u},\eta^*\big)}_{F_j^c\left(\boldsymbol{u},\eta^*\right)} + \underbrace{\left(A^{-1}\right)_{ji} \ b_i^s\big(\boldsymbol{u},\eta^*\big)}_{F_j^s\left(\boldsymbol{u},\eta^*\right)} \ , \tag{11}$$

where $F_j^c\big(\boldsymbol{u},\eta^*\big)$ and $F_j^s\big(\boldsymbol{u},\eta^*\big)$ are the generalized nodal fluxes due to contour integrals and surface integrals, respectively.

In the third step of the wetting-drying method, the generalized nodal fluxes are modified by cancelling out those that are negative in dry areas:

$$\frac{\eta_j^{***}-\eta_j^n}{\Delta t} \quad = \quad F_j^{c*}\big(\boldsymbol{u},\eta^*\big) + F_j^{s*}\big(\boldsymbol{u},\eta^*\big) \ ,$$

$$F_j^{c*} = \begin{cases} 0 & \text{if} \quad F_j^c < 0 \quad \& \quad \eta_j^n + h_j < H_{\text{dry}} \\ F_j^c & \text{otherwise} \end{cases} , \tag{12}$$

$$F_j^{s*} = \begin{cases} 0 & \text{if there is a node } i \in \Omega_e \\ & \quad \text{with} \quad F_j^s < 0 \quad \& \quad \eta_i^n + h_i < H_{\text{dry}} \\ F_j^s & \text{otherwise} \end{cases} . \tag{13}$$

The mass conserving property of the second step is not altered in the third step since we simply cancel out fluxes. Clearly, the algorithm as a whole preserves mass. Moreover, all DG methods are intrinsically locally mass conservative, as we can make a flux balance for each element. Since the only effect of the present wetting-drying is to cancel out some fluxes in dry areas, the method is also locally mass conservative.

There are also a few modifications in equation (2). First of all, the clipped elevation η^* is used to ensure that only positive water depths are dealt with, thus avoiding dividing by zero in some terms. Moreover, for stability reasons, we cancel out the gravity effect within the dry elements [41] to allow the free surface to remain parallel to the bottom. Finally, in shallow areas, we increase the bottom stress and the eddy viscosity, and decrease the surface stress. For this, we use the concept of "buffer" layer [32, 31, 63, 59], the thickness of which is H_{buf}. The terms to increase or decrease are multiplied by a factor linearly varying from 1 when $H \geq H_{\text{buf}}$ to f_{buf} when $H \leq H_{\text{dry}}$. The factor f_{buf} has different values for each term. Inside an element with at least one dry node, the above-mentioned terms are multiplied by f_{buf}, whatever the value of H.

Herein, for the sake of simplicity, the method is presented using an explicit Euler time stepping scheme. Nevertheless, it can be easily transposed to any other explicit scheme, by applying the different steps of the wetting-drying method to each sub-time step. However, all flux-limiting methods are intrinsically nonlinear. As there are conditions to turn on/off a flux, these methods are discontinuous with respect to these variables. It is therefore not possible to deduce a stable linearization of the method as it is, and so implicit time stepping is not available directly.

If there were no wetting-drying to deal with, η^{n+1} would simply be computed using the following equation:

$$\frac{\eta^{n+1} - \eta^n}{\Delta t} = F\big(\eta^n, \boldsymbol{u}\big) , \tag{14}$$

which is just the equation (7) with $\eta^* = \eta^n$ and $F^* = F$, i.e. with no modification of η^n and F during the first and third intermediate steps, respectively. The extra computing cost of the present wetting-drying method is therefore due to these two intermediate steps, which only consist in modifying some nodal values in dry areas and are therefore quite cheap. Moreover, this wetting-drying method does not require additional stabilily constraint, except the conventional CFL stability condition of explicit time marching.

The equations (1) and (2), combined with the above wetting-drying method, are spatially discretized using P_1^{DG} elements for both the elevation and the velocity, the stability being ensured by computing the fluxes at the interface between two triangles

using the values deduced from a Roe solver. This is explained in details by Comblen et al. [19]. For the temporal discretization, an explicit second-order Runge-Kutta scheme is used for most of the terms, while an implicit second-order Runge-Kutta is used for the bottom stress term.

The proposed wetting-drying method is implemented into SLIM [19, 20], which is already successfully used for several applications in the Great Barrier Reef [40, 60, 12, 61], the Scheldt Estuary [22, 23] and Lake Tanganyika [29]. The unstructured meshes used for the test cases and the Scheldt Estuary application are built by means of the open source software GMSH[2] [27, 39].

3 Verification of the method

3.1 Balzano test cases

Balzano [7] presented three simple one-dimensional test cases to compare different flux-limiting wetting-drying methods for finite difference models. These can be used to evaluate the accuracy of other wetting-drying methods [62]. The computational domain of the three test cases is a one-dimensional basin 13800 m in length. However, as the goal of this paper is to verify a wetting-drying method for two-dimensional models, this one-dimensional domain is replaced by a two-dimensional one. This new domain has a relatively large width of 7200 m and frictionless coastlines. The two-dimensional problems and their corresponding one-dimensional Balzano test cases must have the same solutions.

The reference water level is 5 m at the open boundary and zero at the other end, where the basin is closed. The Coriolis force, the surface stress and the horizontal viscosity are not taken into account. The bottom stress is parameterized with the Chézy-Manning-Strickler formulation :

$$\frac{\boldsymbol{\tau}^b}{\rho} = n^2 g \frac{|\boldsymbol{u}|\boldsymbol{u}}{H^{1/3}} , \tag{15}$$

where the Manning coefficient n is equal to 0.02 s/m$^{1/3}$, which is a typical value for sand [30, 31]. Finally, the threshold thickness H_{dry} is fixed to 0.01 m, and because of the relatively low basin slopes for each test case, no modification of terms has to be done in the buffer layer ($f_{\text{buf}} = 1$). These are the features common to the three test cases, which are therefore quite similar. Actually, they only differ in their bathymetry and in their external forcing.

For the first Balzano test case (Figure 2), a basin with a uniform bottom slope is considered. The analytical expression of the bathymetry may be found in Appendix A. At the open boundary, a sinusoidal water level variation is imposed, with a period of 12 h and an amplitude of 2 m, the water depth at the open boundary oscillating

[2] http://www.geuz.org/gmsh

between 3 and 7 m. Following the observations of Balzano, some methods cause undesired wiggles in the free surface profile during the wetting phase. It is clearly not the case here. In dry areas (where the water thickness is theoretically zero), some methods also suffer from pronounced underestimation (negative water thickness) or overestimation (positive water thickness) of the retention volume. With the present method, the water thickness is always positive. So the retention volume is never underestimated. Moreover, the water thickness in dry areas is controlled by the threshold value H_{dry}, which limits the overestimation to very small values.

In the second Balzano test case (Figure 3), the forcing is similar. The only difference lies in the bathymetry of the basin. While the first basin has a uniform slope, the second one contains a small shelf. The analytical expression of the bathymetry may be found in Appendix A. The mesh is designed to represent it exactly. In addition to the wiggling and retention problems already mentioned, Balzano noticed a runoff problem with some methods in this test case. With these methods, the runoff becomes negligible along the shelf at the end of the drying phase, with an important overestimation of the retention volume. And during the wetting phase, a period of newly increasing runoff is observed. This two phase runoff behavior is clearly not plausible. With the method of this paper, the slowing down of the runoff seems quite linear, which is the correct physical behavior.

In the third Balzano test case (Figure 4), the basin contains a small reservoir. The analytical expression of the bathymetry may be found in Appendix A. The external forcing is also different. The elevation of the water is initially set to 2 m, i.e. the water depth is 7 m at the open boundary and 2 m at the other end. A sinusoidal decay is then applied during 6 h (half the sinusoidal period) at the open boundary to decrease the water depth from 7 to 3 m. Afterwards, the water level at the open boundary is kept to 3 m, and the simulation ends after 100 h. Clearly, the surface in the reservoir should asymptotically reach an horizontal plane at the level of the local peak of the bathymetry. The mesh is designed to represent exactly both the analytical bathymetry and the expected elevation in the reservoir. Among the three Balzano test cases, the third is probably the most difficult to tackle. For example, with most of the modified equation methods, the water surface behavior is badly represented. Indeed, with these methods, some water can flow from the reservoir to the rest of the basin, even when the mean surface level inside the reservoir is below the local peak of the bathymetry. After 100 h of simulation, the expected water level is perfectly simulated in the reservoir. The physics does not seem to be altered close to dry areas.

The first Balzano test case is also used to verify the convergence of the method, by evaluating the L^2 error on the elevation after one tidal cycle (Figure 5). The meshes used for this convergence analysis are similar to that of Figure 2a, with various triangle characteristic lengths, the reference solution being computed on a mesh whose triangle characteristic length is 150 m. The convergence rate is estimated to 1.525, while it

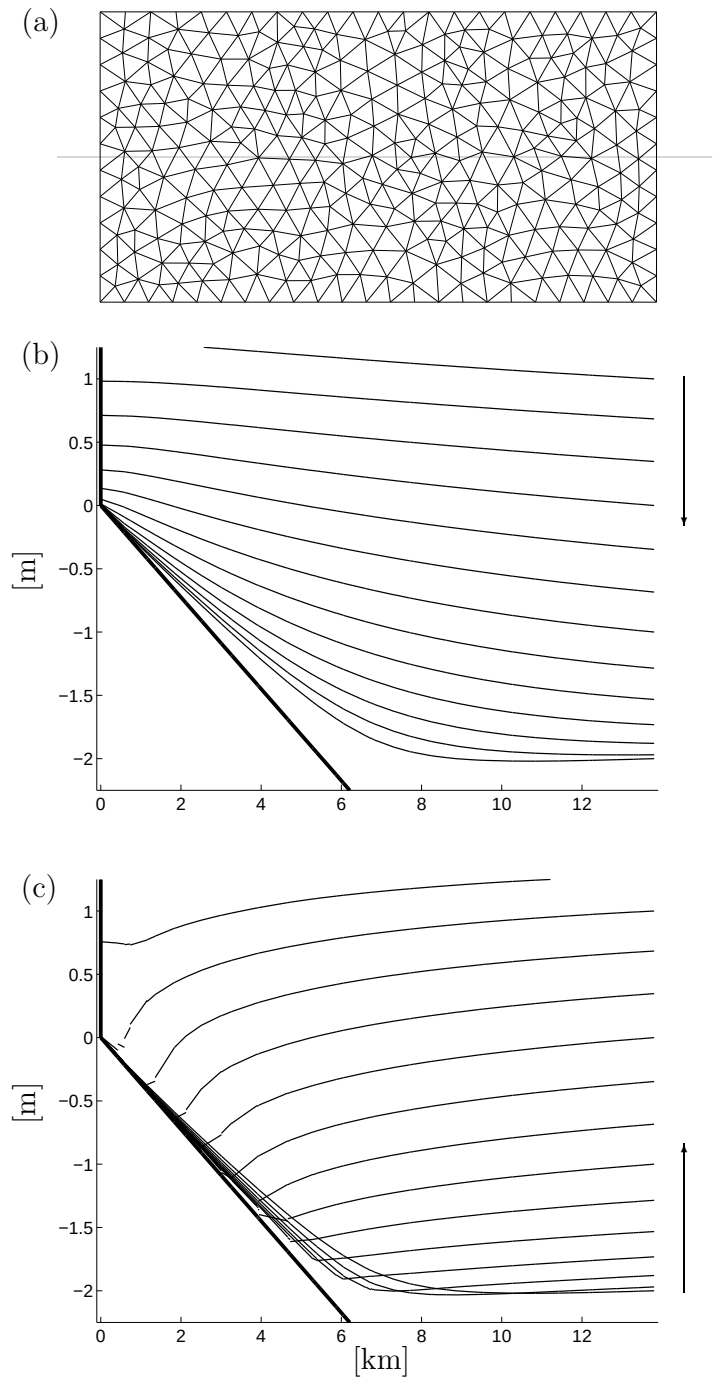

Figure 2: [First Balzano test case] Mesh used, made up with 561 triangles having a characteristic length of 600 m (a); vertical section (gray line of the mesh), through the domain of interest, showing the sea bed (thick line) and the position of the water surface every 20 minutes (thin lines), during the drying (b) and the wetting (c) phases.

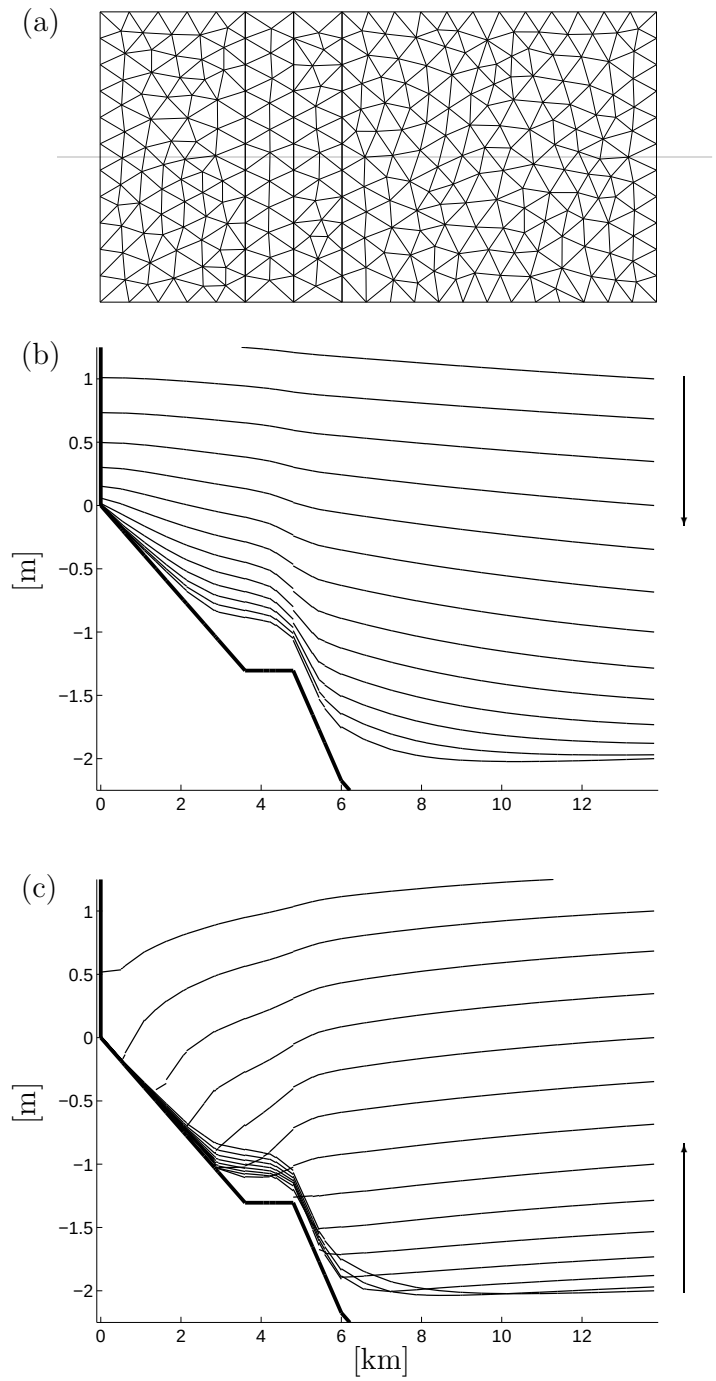

Figure 3: [Second Balzano test case] Mesh used, made up with 557 triangles having a characteristic length of 600 m (a); vertical section (gray line of the mesh), through the domain of interest, showing the sea bed (thick line) and the position of the water surface every 20 minutes (thin lines), during the drying (b) and the wetting (c) phases.

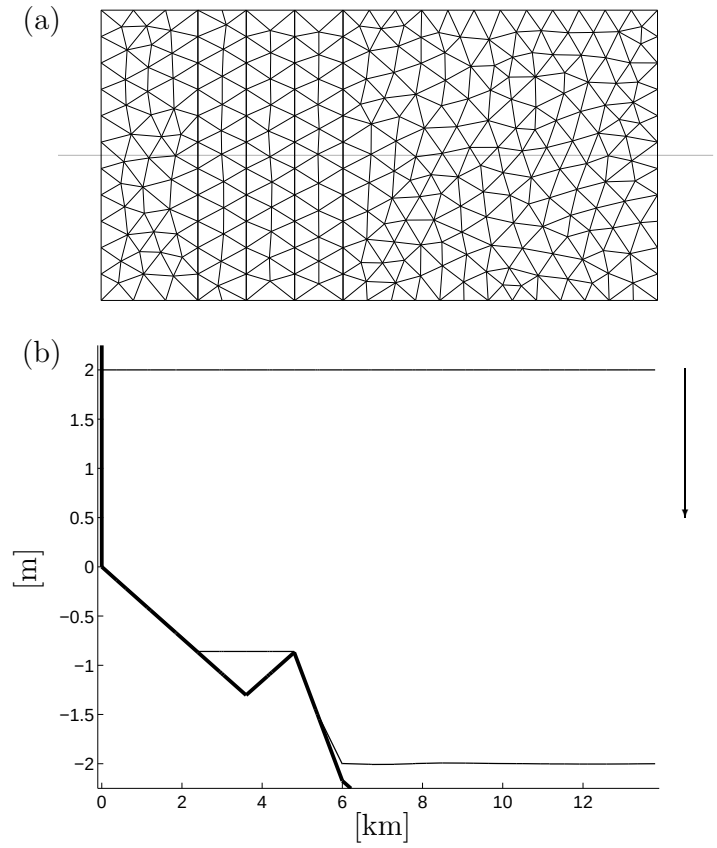

Figure 4: [Third Balzano test case] Mesh used, made up with 543 triangles having a characteristic length of 600 m (a); vertical section (gray line of the mesh), through the domain of interest, showing the sea bed (thick line) and the position of the water surface at initial time and at equilibrium (thin lines) (b).

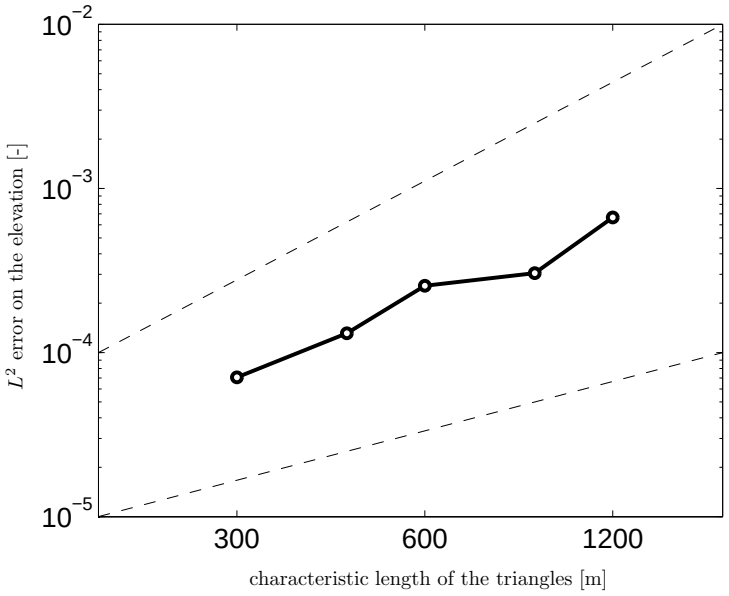

Figure 5: [First Balzano test case] Evolution of the L^2 error on the elevation after 12 h, versus the characteristic length of the triangle meshes; the reference solution is computed on a mesh whose triangle characteristic length is 150 m; the rate of the dashed lines are 1 (below) and 2 (above), while the convergence rate is here estimated to 1.525.

should be theoretically 2 with the $P_1^{DG} - P_1^{DG}$ pair, and without wetting and drying [19]. Actually, the same analysis has been performed for all the test cases: convergence is always observed, and each time at a rate comprised between 1 and 2, the extent of the dry areas decreasing the convergence rate towards 1. This suggests that our wetting-drying method is first order.

3.2 Leclerc test case

Leclerc et al. [41] defined a test case that has been used to verify other wetting-drying methods [31, 34]. In Figure 6, we present the mesh of the domain that is a rectangular basin 100 m wide and 500 m long. Three of the basin edges are coasts, the only open boundary being one of the small edges. All these boundaries are considered frictionless. As in the Balzano test cases, the bathymetry only varies along the length of the basin, but the bottom slope is here much steeper. The analytical expression of the bathymetry may be found in Appendix A. The wetting and drying phenomenon is likely to be more difficult to model due to the steeper slope. However, the threshold thickness H_{dry} is still fixed to 0.01 m, and no modification of terms has to be done in the buffer layer ($f_{\text{buf}} = 1$).

The problem set-up is quite similar to the two first Balzano test cases. The Coriolis

force and the surface stress are not taken into account, but there is here some turbulent viscosity ($\nu = 5$ m^2/s). The Chézy-Manning-Strickler formulation (15) is used to model the bottom stress. The bottom is here a little rougher with a Manning coefficient $n = 0.03$ s/m$^{1/3}$, which is however still typical for sand. A sinusoidal water level variation is imposed at the open boundary, with a period of 1 h and an amplitude of 0.75 m, the water depth at the open boundary oscillating between 0.25 and 1.75 m. The results are in a good agreement with those obtained by Leclerc. They are also similar to the results of Heniche et al. [31] and Jiang and Wai [34], but only outside dry areas, since they used modified equation methods.

3.3 Thacker test case

This last test case, shown in Figure 7, has also been used by Balzano [7] to compare the best methods of its review, and is here of use to illustrate that the method is strictly mass conserving. The domain is a circular closed basin, so that no water can enter or leave the domain; the sea bed is a paraboloid of revolution. At the initial time, the free surface is also a paraboloid of revolution. Then, the free surface moves with free oscillations and wetting and drying occurs on the boundary of the domain. If there is no Coriolis force, no surface stress and no dissipation (neither viscosity nor bottom stress), the analytical solution of the problem is known [56]. The analytical expressions of the bathymetry and the solution of the non dissipative problem may be found in Appendix A.

However, this wetting-drying method requires some dissipation to be stable. The bottom stress is therefore taken into account using the Chézy-Manning-Strickler formulation (15). The values of the wetting-drying parameters are the same as in the former test cases ($H_{\text{dry}} = 0.01$ m and $f_{\text{buf}} = 1$). Several simulations have been run, with various values of the Manning coeffcient n. The evolution of the free surface in the center of the domain is shown on Figure 8. It is clearly seen that, as expected, the model results tend to the Thacker solution when decreasing the Manning coefficient.

Since the method is mass conserving and the domain is closed (and since the flow is incompressible), the total water volume must always remain constant. After four free oscillation cycles, the maximum relative difference between the water volume and its initial value is of the order of 10^{-15}, for each simulation. The volume is therefore strictly conserved, up to round-off errors.

4 Application to the Scheldt Estuary

The Scheldt River flows from Northwestern France, through northern Belgium, ending in the North Sea in the southwestern part of The Netherlands. The area of tidal influence goes up to 160 km from the mouth and includes all the major tributaries. The tidal regime is mainly semi-diurnal (M_2) with mean neap and spring

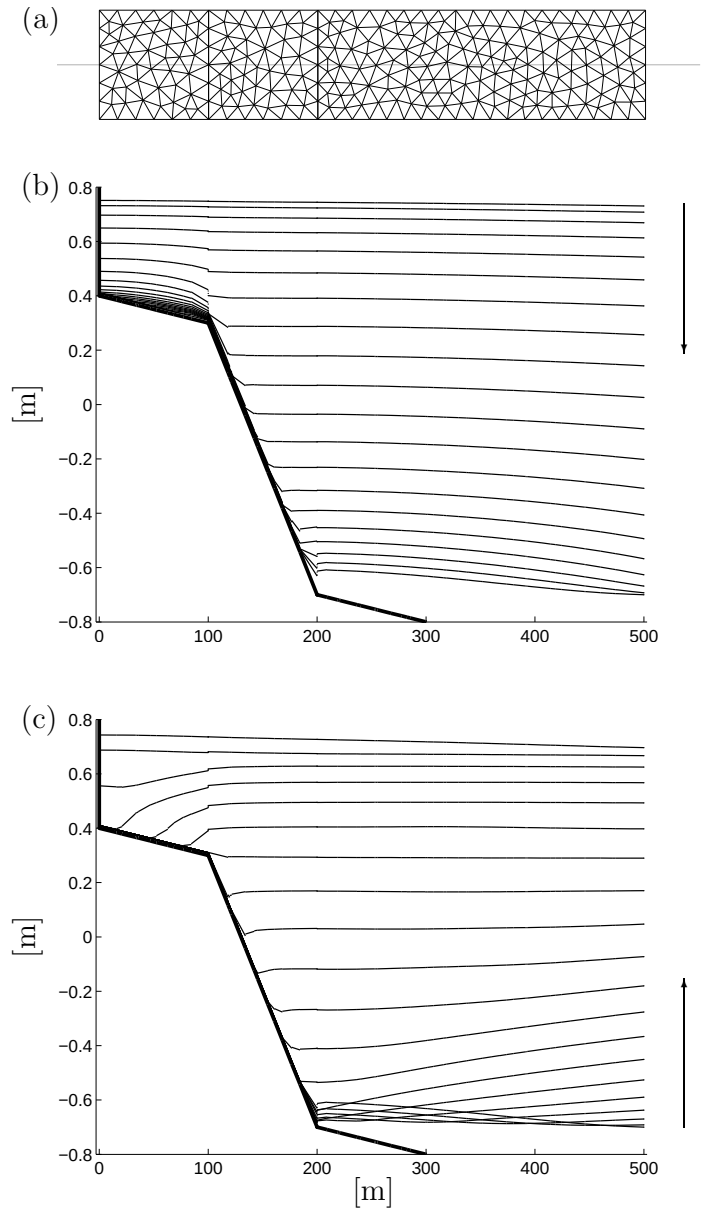

Figure 6: [Leclerc test case] Mesh used, made up with 492 triangles having a characteristic length of 15 m (a); vertical section (gray line of the mesh), through the domain of interest, showing the sea bed (thick line) and the position of the water surface every 90 seconds (thin lines), during the drying (b) and the wetting (c) phases.

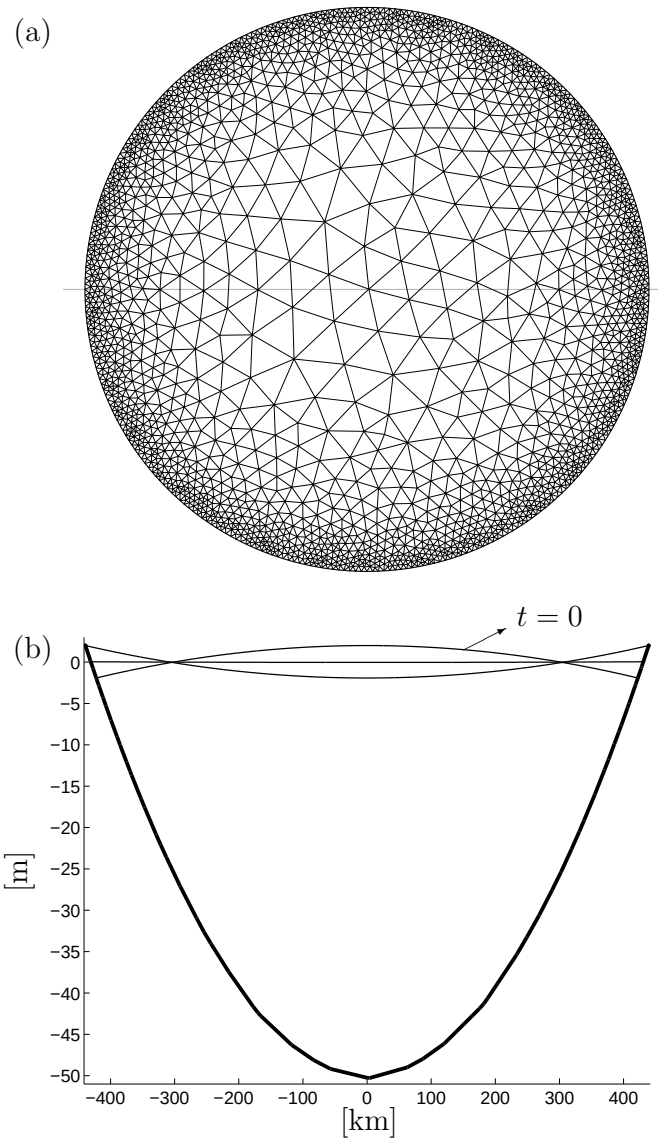

Figure 7: [Thacker test case] Mesh used, made up with 4380 triangles having a characteristic ranging from 10 km (near the border) to 100 km (near the center) (a); vertical section (gray line of the mesh), through the domain of interest, showing the sea bed (thick line) and the position of the water surface (if there is no dissipation) at initial time, after 3 hours and after 6 hours (thin lines) (b).

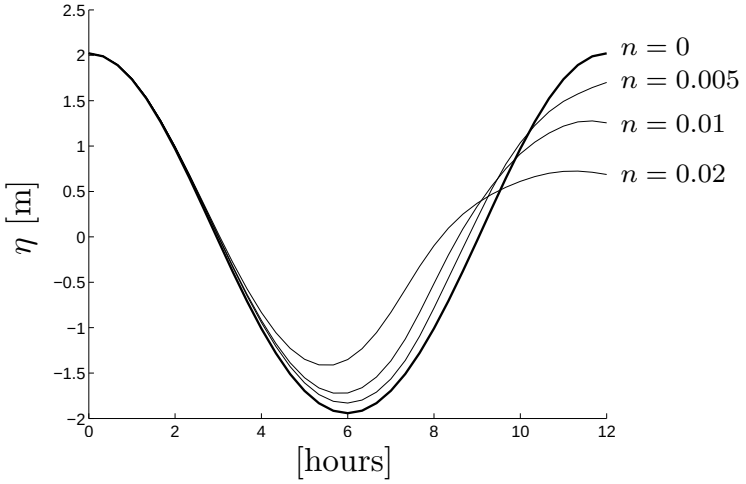

Figure 8: [Thacker test case] Evolution of the free surface in the center of the domain for different values of the Manning coefficient; the thin lines ($n > 0$) are model results, and the thick line ($n = 0$) is the exact solution of Thacker, assuming zero dissipation.

tidal ranges of 2.7 and 4.5 m, respectively. Moreover there is approximately 200 times more water entering the estuary during flood than the averaged water discharge during one M_2 tidal cycle. The Scheldt Estuary may therefore be considered as a macrotidal system. As a consequence, the lower and middle estuary are characterized by a complex morphology with flood and ebb channels surrounding several large tidal flats and salt marshes. Modeling the Scheldt Estuary hydrodynamics requires therefore a wetting-drying method.

As a consequence of the relatively small river discharge and the strong tides, the water column is generally well mixed [57], implying that it is appropriate to use a two-dimensional model to study the Scheldt Estuary. It is therefore a relevant application to test the present two-dimensional wetting-drying method.

The Belgian part of the Scheldt Estuary is situated in a very densely populated area with a very high economic activity, which is strongly conflicting with the high biodiversity values of estuaries [45]. The estuary has been heavily polluted until the mid 1970s, particularly affected by domestic and industrial inputs of large cities such as Brussels, Antwerp, Ghent and their areas, but there is now a progressive improvement of the environmental conditions [54]. Although we mainly focus here on the Dutch part of the estuary, where the main wetting and drying processes take place, it is largely influenced by the upstream polluted Belgian conditions. Modeling the Scheldt Estuary is therefore not only an interesting application to test a wetting-drying method, it is also needed to address important environmental issues.

The computational domain extends to the shelf break and does not cover the Baltic

Sea, ending in the southern Kattegat, the strait between Denmark and Sweden. In the Scheldt, it covers the whole estuarine part, going upstream of Antwerp, 100 km from the mouth. There, the tidal effect is still present and the variables are estimated by means of a one-dimensional model of the Scheldt River (up to Ghent, 160 km from the mouth) and the tributaries that are under tidal influence [23]. The model is here run using a spherical coordinate system [20]. The mesh generated by GMSH on the computational domain of the two-dimensional model is presented in Figure 9.

The bathymetry is based on ETOPO1[3] [5] for the European shelf, and data of the KustZuid model[4] for the Scheldt. The tide is forced at the shelf break using the elevation and velocity harmonics of the global tidal model TPXO7.1[5] [24]. Because they may influence the Belgian/Dutch coastal zone [37], the discharges of the Seine (France), the Thames (United Kingdom), and the Rhine/Meuse (The Netherlands) are also imposed using daily averages from several public data sources[6]. Topological data (cross sections and mean widths, as functions of the water depth) from Projet Mer [38] are used to describle the rivers of the one-dimensional model of the Scheldt River. The discharges of the Scheldt and its tributaries are also imposed using daily averages from a public data source[7].

To represent the boundary layers along the coastlines, we add friction on the coastlines:

$$\nu \frac{\partial u_t}{\partial n} \quad = \quad \alpha u_t \ , \tag{16}$$

where u_t is the velocity component tangential to the boundary, and $\partial/\partial n$ is the derivative in the direction normal to the boundary. A suitable value for α/ν for partial slip along the coasts was found to be 10^{-3} m^{-1}.

In order to incorporate unresolved flow features, the horizontal eddy viscosity is parameterized with the Smagorinsky formulation [53]

$$\nu \quad = \quad c\,\Delta^2 \sqrt{2\left(\frac{\partial u}{\partial x}\right)^2 + 2\left(\frac{\partial v}{\partial y}\right)^2 + \left(\frac{\partial u}{\partial y} + \frac{\partial v}{\partial x}\right)^2} \ , \tag{17}$$

[3] ETOPO1 is a global relief model of Earth's surface from the National Geophical Data Center (http://www.ngdc.noaa.gov/mgg/global/).

[4] Courtesy of M. Zijlema of the National Institute for Coastal and Marine Management (RIKZ), The Hague, The Netherlands.

[5] TPXO7.1 is the current version of a global model of ocean tides, which best-fits, in a least-squares sense, the Laplace Tidal Equations and along track averaged data from TOPEX/Poseidon and Jason (on TOPEX/POSEIDON tracks since 2002) obtained with OTIS (http://www.coas.oregonstate.edu/research/po/research/tide/global.html).

[6] For the Seine, the data are provided by the Groupement d'Intérêt Public (GIP) Seine-Aval (http://seine.aval.crihan.fr/applications_donnees/donnees); for the Thames, the data are provided by the National River Flow Archive (NRFA) (http://www.nwl.ac.uk/ih/nrfa/webdata); and for the Rhine/Meuse, the data are provided by the National Institute for Coastal and Marine Management (RIKZ) and the Institute for Inland Water Management and Waste Water treatment (RIZA) (http://www.waterbase.nl).

[7] For the Scheldt and its main tributaries, the data are provided by the Hydrologic Information Centre (HIC) (http://hydra.vlaanderen.be).

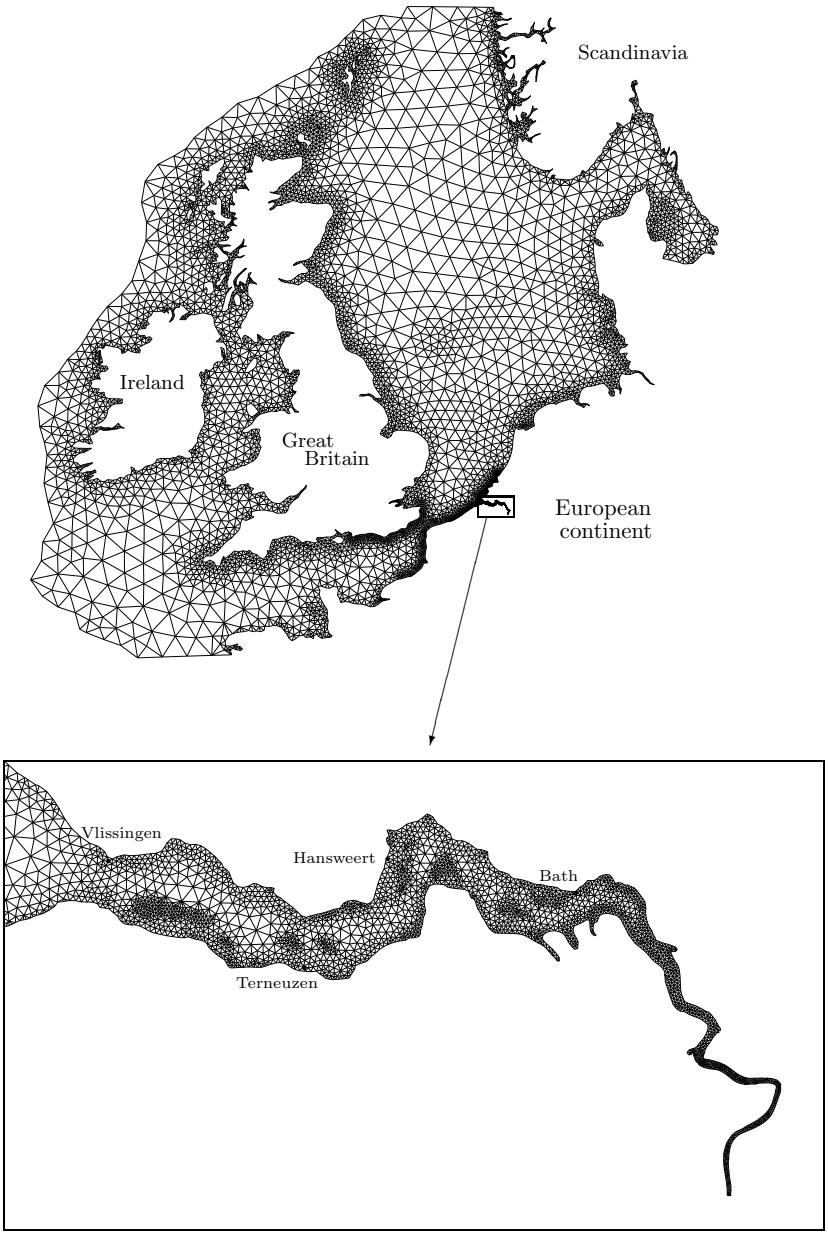

Figure 9: Mesh used for the Scheldt Estuary simulation (15077 triangles); the characteristic length of the triangles is determined following the distance to the coasts and the bathymetry, but also the interest of the area; the mesh size ranges from 200 m (near the upstream boundary in the Scheldt) to 30 km (close to the shelf break and in the deepest parts of the North Sea); black bullets indicate the location of measurement stations where data are available for comparison with model outputs.

where Δ is the characteristic length of the element, and u and v are the components of the velocity in the x and y horizontal directions, respectively. A suitable value of the dimensionless coefficient c for coastal applications is 0.01.

Once again, the Chézy-Manning-Strickler formulation (15), is used to parameterized the bottom stress, with a Manning coefficient n equal to 0.02 $\mathrm{s/m^{1/3}}$. As mentioned earlier, it is a typical value for sand [30, 31].

The surface stress is imposed from NCEP reanalysis data of the wind at 10 m above the mean sea level and of the surface atmospheric pressure[8] [35].

As in the test cases, the threshold thickness H_{dry} is fixed to 0.01 m. However, the Scheldt Estuary is much more difficult to model than the test cases, due to the steep slopes of the bottom. Therefore, in order to stabilize the simulation, we need here to use a buffer layer with a thickness $H_{\mathrm{buf}} = 0.05$ m. Similar value is used by Zheng et al. [63] and Wang et al. [59]. The value of f_{buf} is determined to be 50 for the bottom stress and the viscosity terms, and 10^{-3} for the surface stress term. It has to be pointed out that all the above test cases have also been run with these values of H_{buf} and f_{buf} without altering the quality of the results.

Even if the validation of the model is not the purpose of this paper, a comparison is made between model results and field measurements on different stations. Four of these stations (Bath, Hansweert, Terneuzen and Vlissingen) are located on the Scheldt Estuary (Figure 9) where the wetting and drying processes have a great influence on the hydrodynamics. The fifth station (Vlakte van de Raan) is located a few kilometers upstream of the mouth and is not really influenced by the wetting and drying processes occuring in the estuary. Figure 10 shows a good agreement between the elevation of the free surface computed by the model and the elevation measured at these stations. This is quite convincing since, at this stage, no sensibility analysis has been made on the most important parameters.

Figures 11 and 12 show the water thickness H computed by the model inside the Scheldt Estuary. At high tide (Figures 11a and 12d), deep channels (dark blue) are clearly visible. They allow large ships to sail in order to reach the port of Antwerp. Areas of small depth (light blue) are also distinguished. They are dried during the ebbing phase, when a significant part of the shallow areas becomes dry. These sank banks appear during the ebb tide (Figure 11) and disappear during the rising tide (Figure 12). It would be impossible to model this important hydrodynamic behavior without a specific treatment of the shallow water equations in the dry areas. Our method is therefore working in the vicinity of dry areas. Moreover, Figure 13 shows no transport through dry areas. It is of crucial importance for tracer transport porblems we want to study in the future.

[8] The NCEP Reanalysis data are provided by the NOAA/OAR/ESRL PSD, Boulder, Colorado, USA (http://www.cdc.noaa.gov/cdc/data.ncep.reanalysis.surface.html).

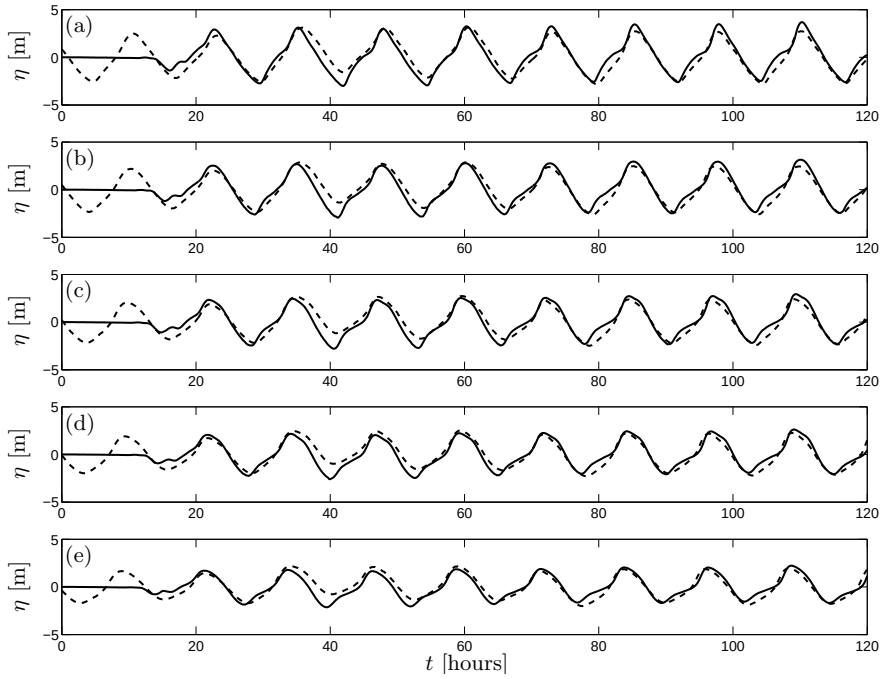

Figure 10: Elevation of the free surface computed by SLIM (plain lines) and measured (dashed lines) at Bath (a), Hansweert (b), Terneuzen (c), Vlissingen (d) and Vlakte van de Raan (e); t is the time elapsed since the beginning of the simulation (June 1, 2001).

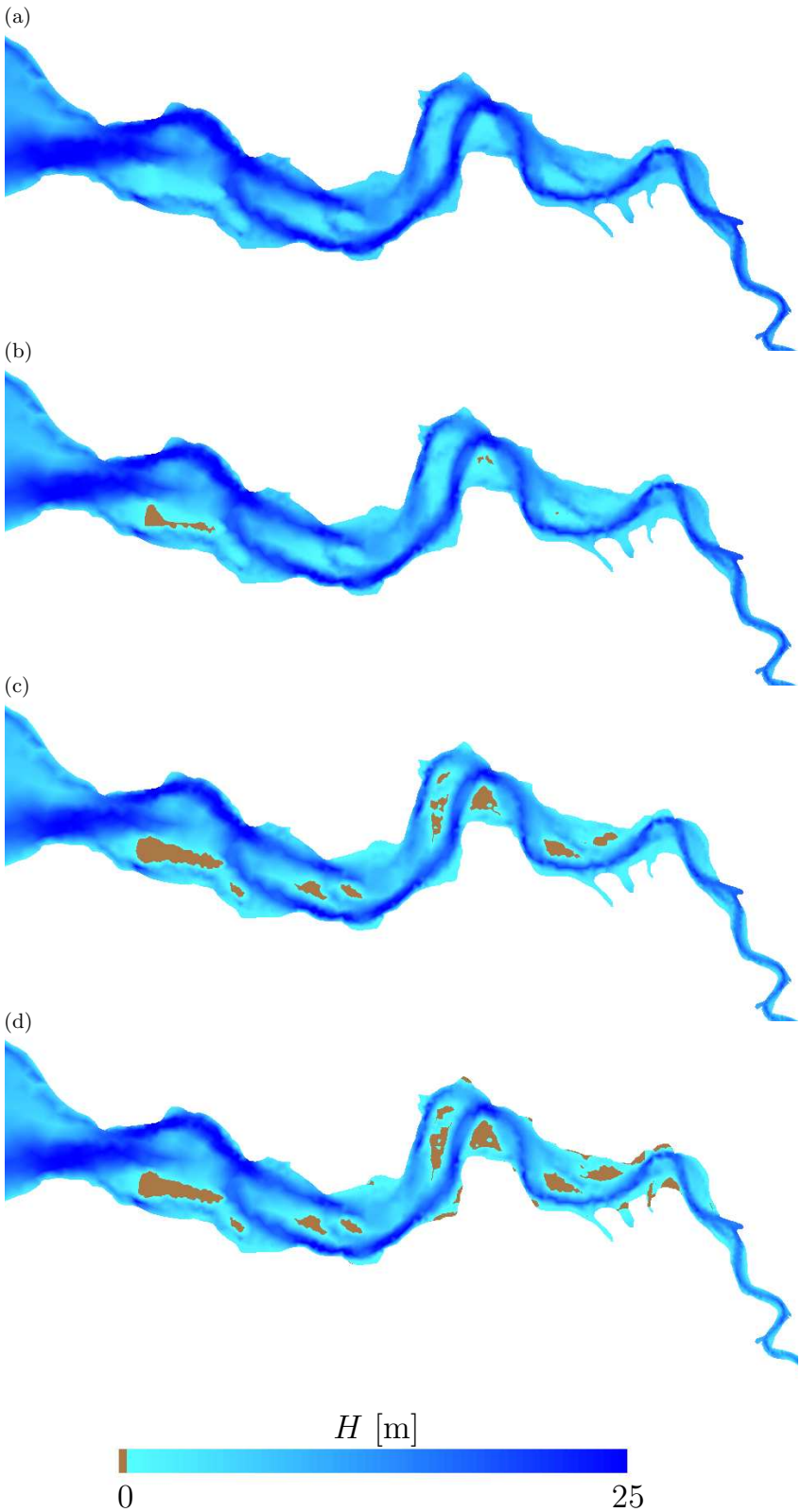

Figure 11: Water thickness H inside the Scheldt Estuary during ebb tide, respectively $\frac{T}{16}$ (a), $\frac{3T}{16}$ (b), $\frac{5T}{16}$ (c) and $\frac{7T}{16}$ after high tide at the mouth (T being the M_2 tidal period); brown areas correspond to dry areas.

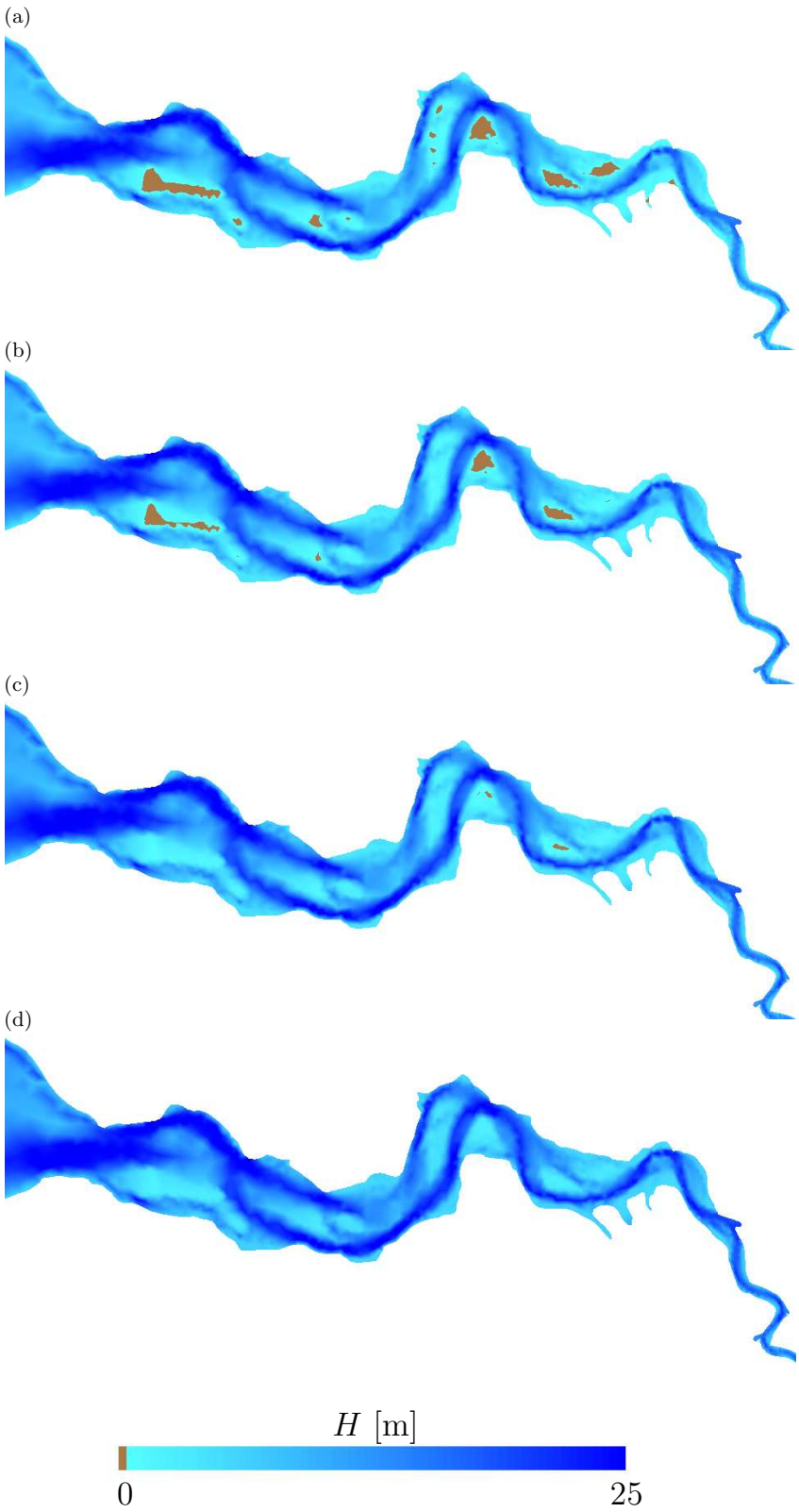

Figure 12: Water thickness H inside the Scheldt Estuary during rising tide, respectively $\frac{9T}{16}$ (a), $\frac{11T}{16}$ (b), $\frac{13T}{16}$ (c) and $\frac{15T}{16}$ after high tide at the mouth (T being the M_2 tidal period); brown areas correspond to dry areas.

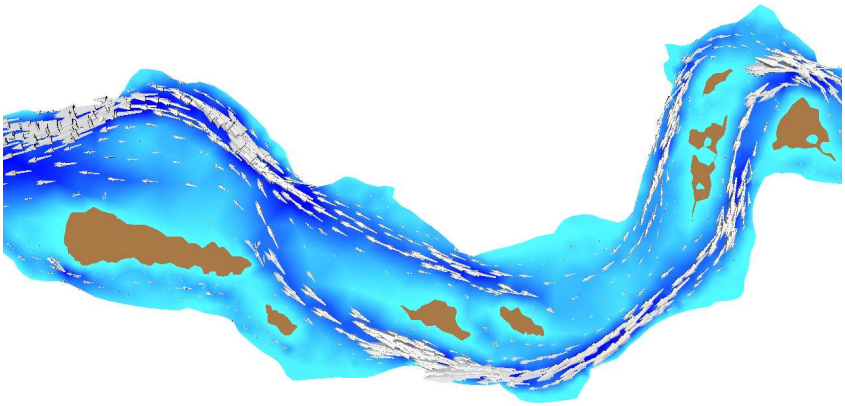

Figure 13: Water thickness inside the Scheldt Estuary $\frac{5T}{16}$ (a) after high tide at the mouth (T being the M_2 tidal period); brown areas correspond to dry areas; the arrows are parallel to the transport $H\boldsymbol{u}$ and their length is proportional to the transport intensity $H|\boldsymbol{u}|$.

5 Conclusion

A flux-limiting wetting-drying method is designed for finite-element shallow-water models using discontinuous linear elements for the elevation. The key ingredient of the method is the use of limiters for generalized nodal fluxes. It is implemented into a model that uses P_1^{DG} elements for all the variables and an explicit second-order Runge-Kutta scheme for most of the terms. The verification is performed by solving successfully several standard problems, namely the Balzano [7] and Leclerc [41] test cases. The Thacker test case [56] is also dealt with to illustrate the important mass conservation property. The method is then used to model the wetting and drying processes occuring in the Scheldt Estuary, shared by Belgium and The Netherlands, where large sand banks are periodically submerged by the tide. We therefore demonstrate the accuracy of the method to describe the hydrodynamics around dry areas. In particular, the method is mass conserving, and there is no transport through dry areas, which is very important when dealing with chemical or biological tracers.

Acknowledgements

Eric Deleersnijder and Richard Comblen are a Research Associate and a Research Fellow, respectively, with the Belgian National Fund for Scientic Research (FNRS). Jonathan Lambrechts is a Research Fellow with the Belgian Fund for Research in Industry and Agriculture (FRIA). The present work was carried out under the auspices of the Interuniversity Attraction Pole TIMOTHY, which is funded by the Belgian Science

Policy under contract IAP6.13. It was also carried out within the scope of the project "A second-generation model of the ocean system", which is funded by the Communauté Française de Belgique, as Actions de Recherche Concertées, under contract ARC 04/09-316. The authors are indebted to Benjamin de Brye (UCL, Louvain-la-Neuve, Belgium) for his contributions to the development of the model, to Sébastien Blaise (UCL, Louvain-la-Neuve, Belgium) for his help in drawing the figures of the Scheldt Estuary, and to Eric Delhez (ULg, Liège, Belgium) for providing useful data.

A Test case analytical expressions

First Balzano test case

$$h = x/2760 \qquad \forall x \ . \tag{18}$$

where x is the coordinate in the main direction of the basin.

Second Balzano test case

$$\begin{cases} h = x/2760 & \text{if } \ x \leq 3600 \text{ m } \text{ , or if } \ x \geq 6000 \text{ m } \ , \\ h = 30/23 & \text{if } \ 3600 \text{ m } \geq x \geq 4800 \text{ m } \ , \\ h = x/1380 - 50/23 & \text{if } \ 4800 \text{ m } \geq x \geq 6000 \text{ m } \ . \end{cases} \tag{19}$$

Third Balzano test case

$$\begin{cases} h = x/2760 & \text{if } \ x \leq 3600 \text{ m } \text{ , or if } \ x \geq 6000 \text{ m } \ , \\ h = -x/2760 + 60/23 & \text{if } \ 3600 \text{ m } \geq x \geq 4800 \text{ m } \ , \\ h = x/920 - 100/23 & \text{if } \ 4800 \text{ m } \geq x \geq 6000 \text{ m } \ . \end{cases} \tag{20}$$

Leclerc test case

$$\begin{cases} h = x/1000 - 0.4 & \text{if } \ x \leq 100 \text{ m } \ , \\ h = x/100 - 1.3 & \text{if } \ 100 \text{ m } \geq x \geq 200 \text{ m } \ , \\ h = x/1000 + 0.5 & \text{if } \ x \geq 200 \text{ m } \ . \end{cases} \tag{21}$$

Thacker test case

The Thacker test case bathymetry is

$$h \ = \ h_0 \frac{R^2 - r^2}{R^2} \ , \tag{22}$$

where r is the distance to the center of the basin, and R and h_0 are the basin radius at rest and the water depth in the center of the basin at rest, respectively.

The analytical expression of the elevation for the non dissipative problem is

$$\eta \ = \ h_0 \left(\frac{\sqrt{1 - A^2}}{1 - A\cos\omega t} - 1 - \frac{r^2}{R^2} \left(\frac{1 - A^2}{(1 - A\cos\omega t)^2} - 1 \right) \right) \ , \tag{23}$$

with

$$\omega^2 = \frac{8gh_0}{R^2} , \tag{24}$$

$$A = \frac{(h_0+\eta_0)^2 - h_0^2}{(h_0+\eta_0)^2 + h_0^2} , \tag{25}$$

where η_0 is the initial elevation of the free surface in the center.

The parameters choosen to obtain a period of oscillations equal to 12 hours are

$$\begin{aligned} R &= 430.62 \text{ km}, \\ h_0 &= 50 \text{ m}, \\ \eta_0 &= 2 \text{ m}. \end{aligned}$$

References

[1] Abualtayef, M., Kuroiwa, M., Tanaka, K., Matsubara, Y., and Nakahira, J. (2008). Three-dimensional hydrostatic modeling of a bay coastal area. *J. Mar. Sci. Technol.*, 13:40–49.

[2] Ainsworth, M. (2004). Dispersive and dissipative behaviour of high order discontinuous Galerkin finite element methods. *J. Comput. Phys.*, 198(1):106–130.

[3] Aizinger, V. and Dawson, C. (2002). A discontinuous Galerkin method for two-dimensional flow and transport in shallow water. *Adv. Water Resour.*, 25(1):67–84.

[4] Aizinger, V. and Dawson, C. (2007). The local discontinuous Galerkin method for three-dimensional shallow water flow. *Comput. Methods Appl. Mech. Eng.*, 196(4-6):734–746.

[5] Amante, C. and Eakins, B. W. (2008). ETOPO1 1 arc-minute global relief model: procedures, data sources and analysis. Technical report, National Geophysical Data Center, NESDIS, NOAA, U.S. Department of Commerce, Boulder, CO.

[6] Arnold, D. N., Brezzi, F., Cockburn, B., and Marini, L. D. (2002). Unified analysis of discontinuous Galerkin methods for elliptic problems. *SIAM J. Numer. Anal.*, 39(5):1749–1779.

[7] Balzano, A. (1998). Evaluation of methods for numerical simulation of wetting and drying in shallow water flow models. *Coast. Eng.*, 34(1-2):83–107.

[8] Begnudelli, L. and Sanders, B. F. (2007). Conservative wetting and drying methodology for quadrilateral grid finite-volume models. *J. Hydraul. Eng.*, 133(3):312–322.

[9] Bernard, P.-E., Chevaugeon, N., Legat, V., Deleersnijder, E., and Remacle, J.-F. (2007). High-order h-adaptative discontinuous Galerkin methods for ocean modelling. *Ocean Dyn.*, 57(2):109–121.

[10] Bernard, P.-E., Deleersnijder, E., Legat, V., and Remacle, J.-F. (2008). Dispersion analysis of discontinuous Galerkin schemes applied to Poincaré, Kelvin and Rossby waves. *J. Sci. Comput.*, 34(1):26–47.

[11] Bernard, P.-E., Remacle, J.-F., and Legat, V. (2009). Boundary discretization for high order discontinuous Galerkin computations of tidal flows around shallow water islands. *Int. J. Numer. Methods Fluids*, 59(5):535–557.

[12] Blaise, S., Deleersnijder, E., White, L., and Remacle, J.-F. (2007). Influence of the turbulence closure scheme on the finite-element simulation of the upwelling in the wake of a shallow-water island. *Cont. Shelf Res.*, 27(18):2329–2345.

[13] Burchard, H., Bolding, K., and Villarreal, M. R. (2004). Three-dimensional modelling of estuarine turbidity maxima in a tidal estuary. *Ocean Dyn.*, 54(2):250–265.

[14] Casulli, V. (2009). A high-resolution wetting and drying algorithm for free-surface hydrodynamics. *Int. J. Numer. Methods Fluids*, 60(4):391–408.

[15] Chevaugeon, N., Xin, J., Hu, P., Li, X., Cler, D., Flaherty, J. E., and Shephard, M. S. (2005). Discontinuous Galerkin methods applied to shock and blast problems. *J. Sci. Comput.*, 22-23(1-3):227–243.

[16] Christian, C. D. and Palmer, G. N. (1997). A deforming finite element mesh for use in moving one-dimensional boundary wave problems. *Int. J. Numer. Methods Fluids*, 25(4):407–420.

[17] Cockburn, B. and Shu, C. (1998). The Runge-Kutta discontinuous Galerkin method for conservation laws V : multidimensional systems. *J. Comput. Phys.*, 141(2):199–224.

[18] Cockburn, B. and Shu, C. (2001). Runge-Kutta discontinuous Galerkin methods for convection-dominated problems. *J. Sci. Comput.*, 16(3):173–261.

[19] Comblen, R., Lambrechts, J., Remacle, J.-F., and Legat, V. (2009a). Practical evaluation of five partly discontinuous finite elments pairs for the non-conservative shallow water equations. *Int. J. Numer. Methods Fluids (in press)*. DOI: 10.1002/fld.2094.

[20] Comblen, R., Legrand, S., Deleersnijder, E., and Legat, V. (2009b). A finite element method for solving the shallow water equations on the sphere. *Ocean Model.*, 28(1-3):12–23.

[21] Dawson, C. and Aizinger, V. (2005). A discontinuous Galerkin method for three-dimensional shallow water equations. *J. Sci. Comput.*, 22-23(1-3):245–267.

[22] de Brauwere, A., De Ridder, F., Gourgue, O., Lambrechts, J., Comblen, R., Pintelon, R., Passerat, J., Servais, P., Elskens, M., Baeyens, W., Kärnä, T., de Brye, B., and Deleersnijder, E. (2009). Design of a sampling strategy to optimally calibrate a reactive transport model: exploring the potential for *Escherichia coli* in the Scheldt Estuary. *Environ. Model. Softw.*, 24(8):969–981.

[23] de Brye, B., de Brauwere, A., Gourgue, O., Kärnä, T., Lambrechts, J., Comblen, R., and Deleersnijder, E. (2009). A finite-element, multi-scale model of the Scheldt tributaries, river, estuary and ROFI. *Coast. Eng. (submitted).*

[24] Egbert, G. D., Bennet, A. F., and Foreman, M. G. G. (1994). TOPEX/POSEIDON tides estimated using a global inverse model. *J. Geophys. Res.*, 99(C12):24821–24852.

[25] Ern, A., Piperno, S., and Djadel, K. (2008). A well-balanced Runge-Kutta discontinuous Galerkin method for the shallow-water equationswith flooding and drying. *Int. J. Numer. Methods Fluids*, 58(1):1–25.

[26] Ertürk, Ş. N., Bilgili, A., Swift, M. R., Brown, T., Çelikkol, B., Ip, J. T. C., and Lynch, D. R. (2002). Simulation of the Great Bay Estuarine System: tides with tidal flats wetting and drying. *J. Geophys. Res.*, 107(C5). DOI : 10.1029/2001JC000883.

[27] Geuzaine, C. and Remacle, J.-F. (2009). GMSH : a finite element mesh generator with built-in pre- and post-processing facilities. *Int. J. Numer. Methods Eng.*, 79(11):1309–1331.

[28] Giraldo, F. X. (2006). High-order triangle-based discontinuous Galerkin methods for hyperbolic equations on a rotating sphere. *J. Comput. Phys.*, 214(2):447–465.

[29] Gourgue, O., Deleersnijder, E., and White, L. (2007). Toward a generic method for studying water renewal, with application to the epilimnion of Lake Tanganyika. *Estuar. Coast. Shelf Sci.*, 74(4):628–640.

[30] Graf, H. and Altinakar, M. S. (1993). *Hydraulique fluviale - Tome 1: Ecoulement permanent uniforme et non uniforme*, volume 16 of *Traité de Génie Civil de l'Ecole polytechnique fédérale de Lausanne*. Presses Polytechniques et Universitaires Romandes, Lausanne, Suisse.

[31] Heniche, M., Secretan, Y., Boudreau, P., and Leclerc, M. (2000). A two-dimensional finite element drying-wetting shallow water model for rivers and estuaries. *Adv. Water Resour.*, 23(4):359–372.

[32] Ip, J. T. C., Lynch, D. R., and Friedrichs, C. T. (1998). Simulation of estuarine flooding and dewatering with application to Great Bay, New Hampshire. *Estuar. Coast. Shelf Sci.*, 47(2):119–141.

[33] Ji, Z.-G., Morton, M. R., and Hamrick, J. M. (2001). Wetting and drying simulation of estuarine processes. *Estuar. Coast. Shelf Sci.*, 53(5):683–700.

[34] Jiang, Y. W. and Wai, O. W. H. (2005). Drying-wetting approach for 3D finite element sigma coordinate model for estuaries with large tidal flats. *Adv. Water Resour.*, 28(8):779–792.

[35] Kalnay, E., Kanamitsu, M., Kistler, R., Collins, W., Deaven, D., Gandin, L., Iredell, M., Saha, S., White, G., Woollen, J., Zhu, Y., Chelliah, M., Ebisuzaki, W., Higgins, W., Janowiak, J., Mo, K. C., Ropelewski, C., Wang, J., Leetmaa, A., Reynolds, R., Jenne, R., and Joseph, D. (1997). The NCEP/NCAR 40-year reanalysis project. *Bull. Am. Meteorol. Soc.*, 77(3):437–471.

[36] Krivodonova, L., Xin, J., Remacle, J.-F., Chevaugeon, N., and Flaherty, J. E. (2004). Shock detection and limiting with discontinuous Galerkin methods for hyperbolic conservation laws. *Appl. Numer. Math.*, 48(3-4):323–338.

[37] Lacroix, G., Ruddick, K. G., Ozer, J., and Lancelot, C. (2004). Modelling the impact of the Scheldt and Rhine/Meuse plumes on the salinity distribution in Belgian waters (southern North Sea). *J. Sea Res.*, 52(3):149–163.

[38] Laforce, E., Wens, F., and Roovers, P. (1977). Mathematical model of the tide area of the Scheldt [Mathematisch model van het tijgebied der Schelde]. WL Rapporten 331-1, Waterbouwkundig Laboratorium, Borgerhout, Belgium. in Dutch.

[39] Lambrechts, J., Comblen, R., Legat, V., Geuzaine, C., and Remacle, J.-F. (2008a). Multiscale mesh generation on the sphere. *Ocean Dyn.*, 58(5-6):461–473.

[40] Lambrechts, J., Hanert, E., Deleersnijder, E., Bernard, P.-E., Legat, V., Remacle, J.-F., and Wolanski, E. (2008b). A multi-scale model of the hydrodynamics of the whole Great Barrier Reef. *Estuar. Coast. Shelf Sci.*, 79(1):143–151.

[41] Leclerc, M., Bellemare, J.-F., Dumas, G., and Dhatt, G. (1990). A finite element model of estuarian and river flows with moving boundaries. *Adv. Water Resour.*, 13(4):158–168.

[42] Leendertse, J. J. (1970). *Principle of computation*, volume 1 of *A water-quality simulation model for well-mixed estuaries and coastal seas.* The Rand Corporation, Santa Monica, California, USA. RM-6230-RC.

[43] Lin, B. and Falconer, R. A. (1997). Three-dimensional layer-integrated modelling of estuarine flows with flooding and drying. *Estuar. Coast. Shelf Sci.*, 44(6):737–751.

[44] Lynch, D. R. and Gray, W. G. (1980). Finite element simulation of flow in deforming regions. *J. Comput. Phys.*, 36(2):135–153.

[45] Meire, P., Ysebaert, T., Van Damme, S., Van den Bergh, E., Maris, T., and Struyf, E. (2005). The Scheldt estuary: a description of a changing ecosystem. *Hydrobiol.*, 540(1-3):1–11.

[46] Nair, R. D., Thomas, S. J., and Loft, R. D. (2005). A discontinuous Galerkin global shallow water model. *Mon. Weather Rev.*, 133(4):876–888.

[47] Oey, L.-Y. (2006). An OGCM with movable land-sea boundaries. *Ocean Model.*, 13(2):176–195.

[48] Prasad, R. S. and Svendsen, I. A. (2003). Moving shoreline boundary condition for nearshore models. *Coast. Eng.*, 49(4):239–261.

[49] Remacle, J.-F., Frazão, S. S., and Shephard, M. S. (2006). An adaptative discretization of shallow-water equations based on discontinuous Galerkin methods. *Int. J. Numer. Methods Fluids*, 52(8):903–923.

[50] Riviere, B. (2008). *Discontinuous Galerkin methods for solving elliptic and parabolic equations: theory and implementation*, volume 35 of *Frontiers in Mathematics*. SIAM.

[51] Schwanenberg, D. and Harms, M. (2004). Discontinuous Galerkin finite-element method for tanscritical two-dimensional shallow water flow. *J. Hydraul. Eng.*, 130(5):412–421.

[52] Sielecki, A. and Wurtele, M. G. (1970). The numerical integration of the nonlinear shallow-water equations with sloping boundaries. *J. Comput. Phys.*, 6(2):219–236.

[53] Smagorinsky, J. (1963). General circulation experiments with the primitive equations. *Mon. Weather Rev.*, 91(3):99–164.

[54] Soetaert, K., Middelburg, J. J., Heip, C., Meire, P., Van Damme, S., and Maris, T. (2006). Long-term change in dissolved inorganic nutrients in the heterotrophic Scheldt estuary (Belgium, The Netherlands). *Limnol. Oceanogr.*, 51(1, part 2):409–423.

[55] Tao, J., Li, Q., Falconer, R. A., and Lin, B. (2001). Modelling and assessment of water quality indicators in a semi-enclosed shallow bay. *J. Hydraul. Res.*, 39(6):611–617.

[56] Thacker, W. C. (1981). Some exact solutions to the nonlinear shallow-water wave equations. *J. Fluid Mech.*, 107:499–508.

[57] Vanderborght, J.-P., Folmer, I. M., Aguilera, D. R., Uhrenholdt, T., and Regnier, P. (2007). Reactive-transport modelling of C, N, and O_2 in a river-estuarine-coastal zone system: Application to the Scheldt estuary. *Mar. Chem.*, 106(1-2):92–110.

[58] Vreugdenhil, C. B. (1994). *Numerical methods for shallow-water flow*, volume 13 of *Water Science and Technology Library*. Kluwer Academic Publishers, Dordrecht, The Netherlands.

[59] Wang, B., Fringer, O. B., Giddings, S. N., and Fong, D. A. (2008). High-resolution simulations of a macrotidal estuary using SUNTANS. *Ocean Model.*, 26(1-2):60–85.

[60] White, L. and Deleersnijder, E. (2007). Diagnoses of vertical transport in a three-dimensional finite element model of the tidal circulation around an island. *Estuar. Coast. Shelf Sci.*, 74(4):655–669.

[61] White, L., Deleersnijder, E., and Legat, V. (2008). A three-dimensional unstructured mesh finite element shallow-water model, with application to the flows around an island and in a wind-driven, elongated basin. *Ocean Model.*, 22(1-2):26–47.

[62] Yuan, D., Lin, B., and Falconer, R. (2008). Simulating moving boundary using a linked groundwater and surface water flow model. *J. Hydrol.*, 349(3-4):524–535.

[63] Zheng, L., Chen, C., and Liu, H. (2003). A modeling study of the Satilla River Estuary, Georgia. I: Flooding-drying process and water exchange over the Salt March-Estuary-Shelf complex. *Estuaries*, 26(3):651–669.

List of Figures